SCIENTIFIC REPORTS

SUBJECT AREAS:
SUPER-RESOLUTION MICROSCOPY
PROTEIN-PROTEIN INTERACTION NETWORKS
HIGH-THROUGHPUT SCREENING
ELECTRON MICROSCOPY

Received
12 July 2012

Accepted
7 February 2013

Published
25 February 2013

Correspondence and requests for materials should be addressed to V.M. (manivel@icgeb.res.in) or K.V.S.R. (kanury@icgeb.res.in)

# Characterizing virulence-specific perturbations in the mitochondrial function of macrophages infected with *mycobacterium tuberculosis*

Shilpa Jamwal[1,2], Mukul Kumar Midha[1,2], Hirdya Narain Verma[2], Atanu Basu[3], Kanury V. S. Rao[1] & Venkatasamy Manivel[1]

[1]Immunology Group, International Centre for Genetic Engineering and Biotechnology, Aruna Asaf Ali Marg, New Delhi – 110067, India, [2]School of Life Sciences, Jaipur National University, Jaipur – 302025, India, [3]National Institute of Virology, Dr. Ambedkar Road, Pune – 411001, India.

**To probe how the pathogen *Mycobacterium tuberculosis* controls host cellular death pathways, we compared mitochondrial responses in human macrophages infected either with the avirulent mycobacterial strain H37Ra, or its virulent counterpart H37Rv. Following H37Ra infection, induction of the apoptotic response was foreshadowed by the early suppression of stress-induced mitochondrial activity. In contrast, mitochondria in H37Rv-infected cells displayed robust activity with increased membrane potential and ATP synthesis. An examination of the mitochondrial proteome revealed that attenuation of mitochondrial function was also coupled with the vigorous activation of bactericidal mechanisms in H37Ra-infected cells. In contrast, augmentation of mitochondrial activity by H37Rv enabled manipulation of host cellular mechanisms to inhibit apoptosis on the one hand, while ensuring fortification against anti-microbial pathways on the other. These results thus provide novel insights into the molecular interplay that facilitates adaptation of virulent mycobacteria within the hostile intracellular milieu of the host macrophage.**

*Mycobacterium tuberculosis* (Mtb) is a highly successful pathogen that has managed to latently infect over one-third of the world's human population. In addition it also causes several million deaths each year. Infection is transmitted through inhalation of aerosolized bacilli, whereupon the Mtb is then taken up by the alveolar macrophages. The success of Mtb as a pathogen lies in its ability to manipulate the hostile intracellular environment of these phagocytic cells. For example, it interferes with the maturation of phagosomes by inhibiting both their acidification and eventual fusion with lysozomes[1–3]. Similarly, other host cellular response pathways such as antigen presentation and the activation of anti-microbial activities are also inhibited[4].

Manipulation of processes linked to cell death is another important strategy that Mtb employs, although the underlying mechanisms and their implications continue to be debated in the literature. For instance, it has long been held that initiation of apoptosis by the infected macrophage is a default pathway that ultimately proves beneficial to the host. This is because apoptotic macrophages are able to contain bacteria until they are eventually killed by effector molecules associated with the programmed cell death process, or are scavenged by other activated phagocytes[5]. Such an interpretation was supported by earlier findings that apoptosis, but not necrosis, of infected macrophages was coupled with killing of the intracellular bacilli[6]. More recent studies in zebrafish, however, suggest that apoptosis may in fact promote bacterial proliferation during granuloma formation[7]. Experiments in at least this model system revealed that phagocytosis of bacterial contents of apoptotic macrophages by newly recruited macrophages enabled subsequent bacterial proliferation, and consequent expansion of granulomas[7,8]. Significantly, this mechanism was found to account for nearly all of the granuloma expansion seen here[7]. In this context the prevailing uncertainty on the mode of host cell death induced by virulent Mtb is also an issue that awaits clarification.

While results have varied with the experimental system employed, cumulative evidence seems to suggest that - at a low to moderate multiplicity of infection (MOI) - the host cell apoptotic response to a virulent Mtb strain is significantly reduced in comparison to that induced by an avirulent strain[9–14]. This capacity of virulent strains to inhibit the apoptotic response was shown to result from the combined effects of induction of anti-apoptosis genes

in the host cell, as well as through the inhibition of apoptosis-inducing signaling pathways[14]. Notably though, the effect of virulent Mtb on host cell death appears to be variable, depending both on MOI and the duration of exposure[12]. Thus, in these experiments, infection of macrophages with the Mtb Erdman strain at an MOI $> 25$ induced apoptosis much like BCG when inoculated at a similar load. In both instances, apoptosis rapidly progressed to secondary necrosis although this process was relatively faster in the case of cells infected with the virulent strain[12]. Interestingly, induction of this death pathway involved a threshold of intracellular bacillary load ($\sim$18 bacilli/macrophage)[11], and was independent of caspase as well as at least some of the cathepsins[15,16,6,13]. In contrast to the ability to inhibit host cell apoptosis at low-to-moderate MOIs, virulent Mtb also secretes proteins that can induce apoptosis of the macrophage. Examples of such proteins include ESAT-6, 19-kDa glycolipoprotein, PE-PGRS33, 38 kDa lipoprotein, and the heparin-binding hemagglutinin protein (HBHA)[15,17–20,7,8]. It has, therefore, been suggested that multiple death pathways operate simultaneously in Mtb-infected macrophages[12]. The mechanism of death that then ultimately dominates probably depends upon variables such as the strain/isolate of Mtb used, and the nature of the host cell employed[12,14].

While the eventual induction of necrosis is key to the pathogenesis of tuberculosis[8], the early suppression of host cellular apoptotic pathways also constitutes an important trait of virulent Mtb. This is evidenced from the fact that infection with an avirulent strain leads to the rapid induction of apoptosis in the host macrophage[21]. Gan et al.[22] have recently delineated the perturbations caused by virulent Mtb, in the terminal events of apoptosis. They demonstrated that, after infection with virulent Mtb, macrophages were unable to develop the cross-linked network of annexin I on their surface. This network is essential for maintaining impermeability of the plasma membrane in apoptotic cells[22]. Interestingly, this block in annexin I crosslinking was found to be Mtb-dependent, and was mediated through the proteolytic cleavage of annexin I[22].

Thus at least some information on the mechanisms by which virulent Mtb interferes with host cell death pathways are now beginning to emerge. However, given the multiplicity and redundancy of pathways involved at the level of both pathogen[12] and the host cell[23], we reasoned that effective manipulation of the programmed cell death pathway would also likely require the pathogen to intervene in the early steps of this process. Further, in view of the central role that mitochondria play in this process[24], an examination of the early perturbations in mitochondrial function induced by Mtb seemed warranted.

In this study, therefore, we compared the consequences of infecting human macrophages with either the avirulent Mtb strain H37Ra, or its virulent counterpart H37Rv. As expected, cells infected with H37Ra eventually underwent apoptosis whereas the frequency of apoptotic cells was significantly reduced in the case of H37Rv infection. Interestingly, this distinction in outcome also correlated with early differences in the manner in which the function of host cell mitochondria were affected. Whereas the mitochondria in cells infected with H37Rv were found to be in a state of increased activity, those in H37Ra-infected cells showed signs of exhaustion. This was evidenced at the level of ultrastructure, membrane potential, and ATP production by the mitochondria. A preliminary mass spectrometric analysis revealed that H37Ra and H37Rv induced quantitatively distinct perturbations in the mitochondrial proteome. More importantly, a functional analysis of these differentially affected proteins enabled rationalization of the divergent host cellular outcomes that were induced in response to infection with these two strains. These results thus suggest that, in contrast to avirulent mycobacteria, virulent Mtb specifically augments functioning of host cell mitochondria in the early stages of infection. It is this heightened activity then that guides a coordinated set of responses that simultaneously inhibit apoptosis and the activation of anti-microbial pathways on the one hand, while also providing a secure niche for mycobacterial survival on the other. Thus an interrogation of early mitochondrial perturbations provides additional insights into the nature of the interplay between host and pathogen.

## Results

**Infection with H37Ra versus H37Rv causes distinct perturbations in host cellular mitochondrial ultrastructure and function.** In this study, we employed the human monocytic THP-1 cells after first differentiating them with PMA. Differentiated cells were subsequently infected either with H37Ra or H37Rv at an MOI of 10 (Methods), and then monitored for any changes in the ultrastructure of the host cell mitochondria by transmission electron microscopy (TEM). While infection-induced alterations were evident as early as 12 hr after infection these changes, however, were more prominent by 24 hr. At this time, the mitochondria in H37Ra-infected cells showed marked alterations in both architecture and appearance. In comparison with the mitochondria in uninfected cells (Fig. 1A and 1B), those in H37Ra-infected cells were characterized by a significant reduction in the electron density of the matrix (Fig. 1C). However, outlines of the cristae were distinct and there was no gross pathology of the mitochondria (Fig. 1D). Such mitochondrial ultrastructure has been previously shown to typify an exhausted state, which also reflects the activation of apoptotic pathways[25].

In contrast to the situation with H37Ra, the mitochondria in THP-1 cells infected with H37Rv displayed increased electron density, with a clear and vivid definition of the cristae (Fig. 1E and 1F). Examination of over 50 cell profiles by TEM further revealed that these mitochondria were relatively more elongated, and showed a tendency to aggregate around Mtb containing phagosomes (Fig. 1E). In addition, direct physical interaction between many of the individual mitochondria could also be seen (see Fig. 1F). Electron tomographic 3D imaging of such representative fields revealed distinct ultrastructural evidence of inter-mitochondrial fusion and contiguous nature of the outer membrane (Fig. 2).

Previous studies have shown that an increase in the electron density of mitochondria, and in the extent of inter-mitochondrial interactions leading to fusion, reflects an augmentation in the functional activity of these mitochondria[26–28]. Consistent with such an interpretation, we found that the mitochondrial membrane potential was significantly increased in H37Rv-infected cells relative to that in cells infected with H37Ra (Fig. 3). Further, this was also true of the ATP to ADP ratio (Fig. 4A). Thus, while a pronounced increase in this ratio was obtained in H37Rv-infected cells, infection with H37Ra caused a significant decrease relative to the corresponding value in uninfected cells (Fig. 4A). That is, whereas the virulent Mtb strain augments activity of the mitochondrial electron transport chain in host cells, its avirulent counterpart inhibits this process.

That the differential effects on mitochondrial activity, caused by H37Ra versus H37Rv infection, indeed enforced distinct outcomes at the level of the host cell response could subsequently be verified by a TUNEL assay that was performed at 72 hrs post-infection. H37Ra infection resulted in a near five-fold increase in the extent of dying cells, when compared to the level of spontaneous apoptosis occurring in uninfected THP-1 cells (Fig. 4B). In contrast to this, the cell death response was only marginally increased in the case of H37Rv-infected cells (Fig. 4B). Importantly, H37Ra-induced death was inhibited by addition of the pan-caspase inhibitor Z-VAD-FMK (Fig. 4B), implicating an apoptotic mode of cell death. In contrast, the pan-caspase inhibitor had no significant effect on H37Rv-infected cells (Fig. 4B). The induction of apoptosis by H37Ra could be further confirmed by the fact that infected cells from Figure 4B also stained positive for annexin-V (Fig. 4C). This, however, was not the case for H37Rv-infected cells where no significant staining for

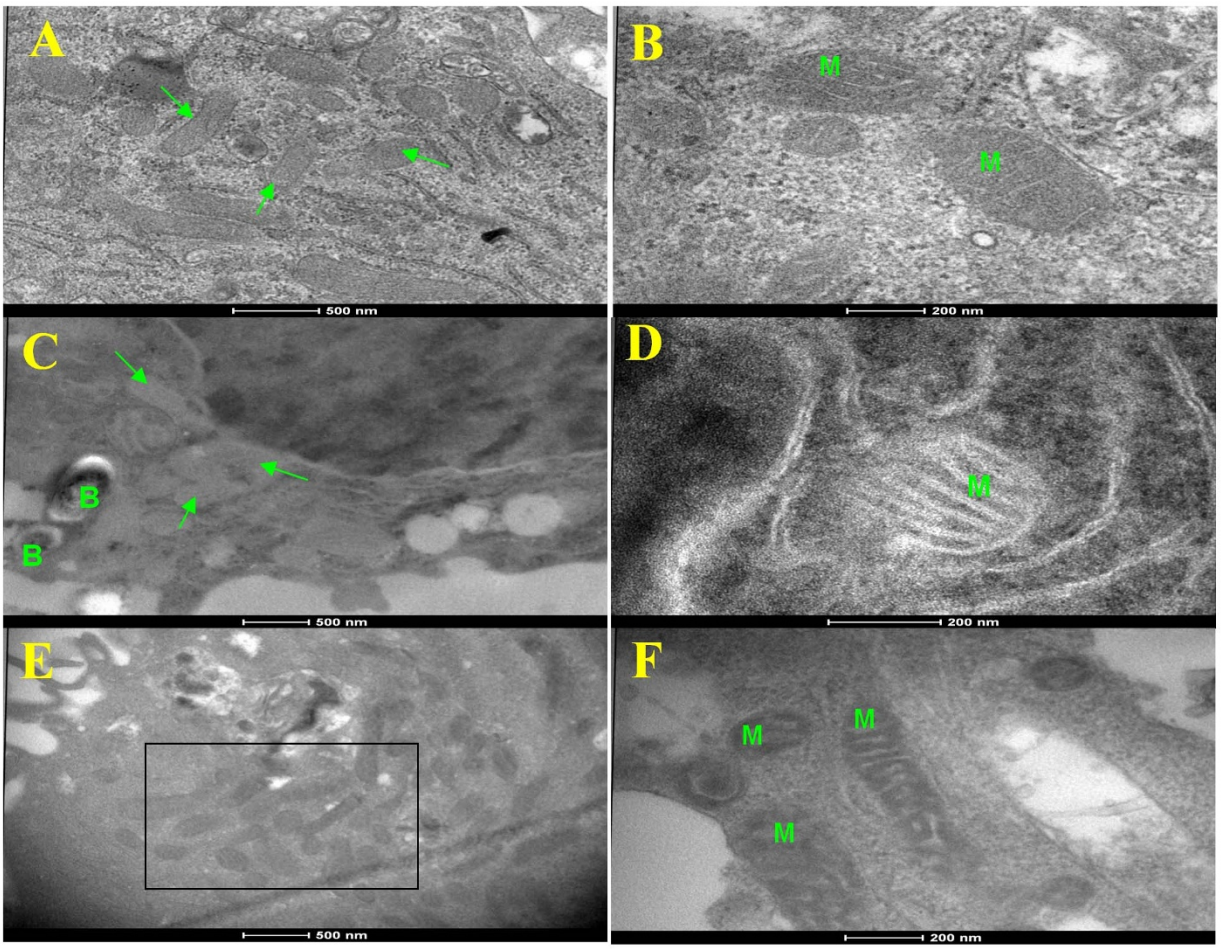


**Figure 1 | Mtb-induced ultrastructural changes in the mitochondria of THP-1 cells.** Figure shows representative transmission electron micrographs of mitochondrial morphology in uninfected THP-1 cells (panels A and B), and in cells infected for 24 hrs either with H37Ra (C,D), or with H37Rv (E,F). In the latter cases, the intracellular bacteria are denoted as 'B' (panels C and E). Whereas uninfected cells show normal mitochondria, those in H37Ra infected cells showed changed ultrastructure (panels C and D). In H37Rv infected cells, however, the mitochondria were electron dense and elongated (see box in panel E) with prominent cristae (panel F). Mitochondria in panels B, D, and F are denoted as 'M'' (scale bar 200 nm), whereas they are identified by arrows in panels A and C. Scale bar for panels A, C, and E is 500 nm.

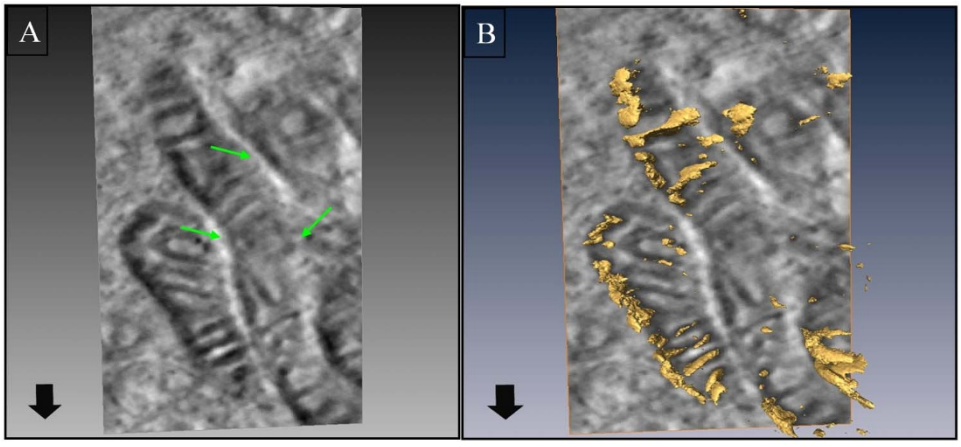


**Figure 2 | Mitochondrial clustering in cells infected with H37Rv imaged by electron tomography.** Panel A shows clustering of mitochondria in H37Rv infected cells. Inter-mitochondrial fusion of (shown by arrows) is clearly evident, suggesting an enhanced interaction between the individual mitochondria. A representative 3D reconstruction of the mitochondria from tomography data sets showing breaches in the mitochondrial cell wall and cristae (arrow) is shown in panel B.

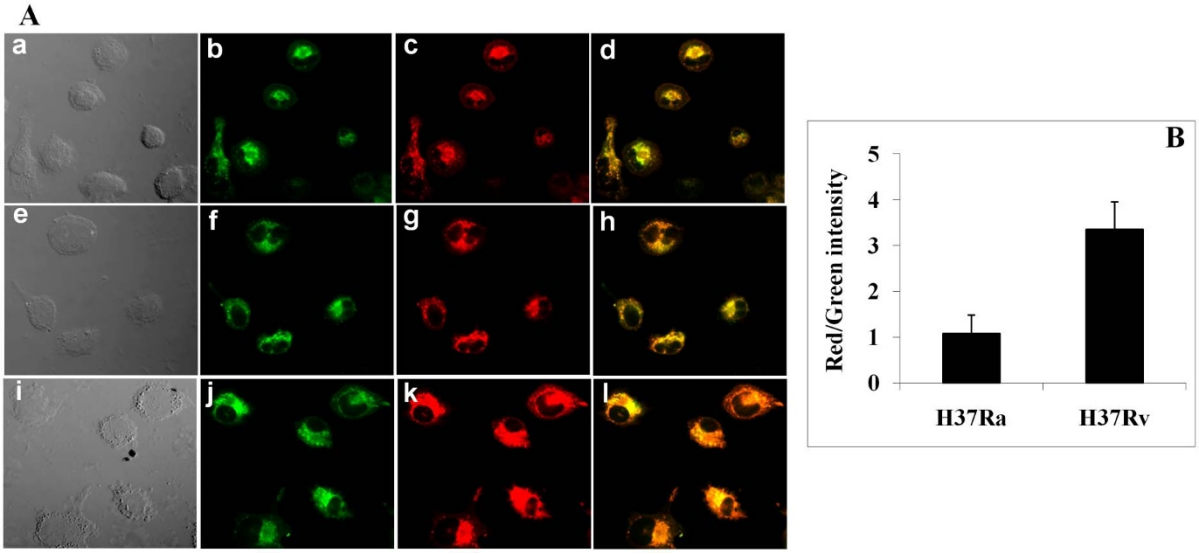


**Figure 3 | Infection with H37Rv causes an increase in the mitochondrial membrane potential.** Cells infected for 24 hrs with either H37Ra or with H37Rv were stained with the lipophilic cationic dye JC1. This dye is commonly used to detect changes in the mitochondrial membrane electrochemical potential in living cells, which is measured as the ratio of the aggregated (red fluorescence) to the monomeric (green fluorescence) forms. Cells were examined by confocal microscopy and the resulting images obtained are shown in Panel A. Here subpanels a-d are images obtained for uninfected cells, whereas e-h and i-l are those obtained for H37Ra and H37Rv infected cells respectively. Subpanels a, e, and i show the DIC images; b, f, and j the distribution of monomeric JC1; and c, g, and k the aggregated form of JC1. A merge of the green and red fluorescence images in shown in subpanels d, h and l. Panel B gives the results of a quantitative analysis of the red/green ratio in H37Ra- versus H37Rv-infected. In both instances, the values are expressed as a ratio of that obtained in uninfected cells and are the mean (± S.E.) of at least 50 cells examined in each case.

annexin-V could be seen. Instead, we detected a low but significant frequency of necrotic cells that could be identified by staining with a membrane impermeable nuclear probe (Fig. 4D). These results, therefore, are consistent with earlier findings that whereas macrophages infected with avirulent Mtb undergo apotosis, this process is suppressed in the case of cells infected with virulent strains[11,29,12]. Thus, our findings in Figures 1 and 2 reveal that H37Ra and H37Rv infection cause distinct perturbations in the host cell mitochondria. Further, it is these differences that then likely account for the differential extent of induction of host cell apoptosis in the two cases. Therefore, we reasoned that a further interrogation of the disparate effects on mitochondria could provide at least some insights into how H37Ra and H37Rv differentially influence the host cell apoptotic response.

**H37Ra and H37Rv induce quantitatively distinct changes in the mitochondrial proteome.** To explore the basis of differential perturbations in function seen above, we next probed for any Mtb-induced changes in the proteome composition of the THP-1 cell mitochondria. We employed the SILAC strategy[30], which was then combined with a 2D LC-MS/MS analysis (Methods). SILAC labeled cells were infected either with H37Ra or with H37Rv. At 24 hours later, equal numbers of infected cells were pooled along with an equal number of uninfected, unlabeled cells. Mitochondria were then isolated from this pooled set, and the extracted proteins subjected to proteolytic digestion followed by 2D LC-MS/MS mass spectrometric analysis (Methods). From replicate samples a total of 1299 unique proteins (Supplementary Table 1) could be identified, of which 295 were those known to be associated either with the mitochondria, or with the MAM (Supplementary Table 2). The relative levels of the majority of these proteins were found to be significantly altered by Mtb infection. Further, differential effects of H37Ra versus H37Rv infection were also clearly evident. As a preliminary analysis, however, we shortlisted only those mitochondrial proteins whose levels were either increased or decreased by 10-fold relative to that in uninfected cells. While this was admittedly a very stringent selection criterion, our goal in this pilot study was simply to assess whether changes in at least some of the components of the mitochondrial proteome indeed signaled the distinct cellular apoptotic response outcomes seen in Figure 4. A total of 16 such proteins were identified with this cut-off and they are listed in Table 1. Of these, expression levels of six were upregulated, whereas those of an additional six were downregulated in H37Rv infected cells. As opposed to this, infection with H37Ra led to an enhancement in relative concentrations of four proteins, along with the suppressed expression of an additional set of five proteins (Table 1). To then examine how these alterations may relate to possible modulations in mitochondrial function, we next sourced the literature for information on their individual functions and these are described below.

**Mitochondrial proteins affected by H37Rv infection.** As described earlier, of the sixteen shortlisted mitochondrial proteins, levels of six were markedly increased in H37Rv-infected cells whereas that of an additional six was suppressed. Concentrations of the remaining four proteins remained relatively unperturbed at least on the basis of our selection criterion (Table 1). The upregulated proteins included HCLS1, ACSL1, VDAC2, ATP50, PRDX1, and ATAD3A. Of these, HCLS1 is the hematopoietic cell-specific Lyn substrate protein. This protein functions as substrate of receptor-coupled tyrosine kinases and is thought to play a role in antigen receptor signaling. While its role in regulating mitochondrial function is not yet known, our present results would suggest that investigations in this direction could likely prove fruitful.

ACSL1, on the other hand, is the Long-chain-fatty acid-CoA ligase that regulates the conversion of free long-chain fatty acids into fatty acyl-CoA[31]. Thereby, this enzyme plays a key role in both lipid biosynthesis and fatty acid catabolism. ACSL1 mRNA levels are increased in cells under both lipogenic and oxidative conditions and this increase has been shown to increase synthesis of phospholipids especially phosphatidylethanolamine and phosphatidylinositol[32]. Maintenance of the functional integrity of mitochondria

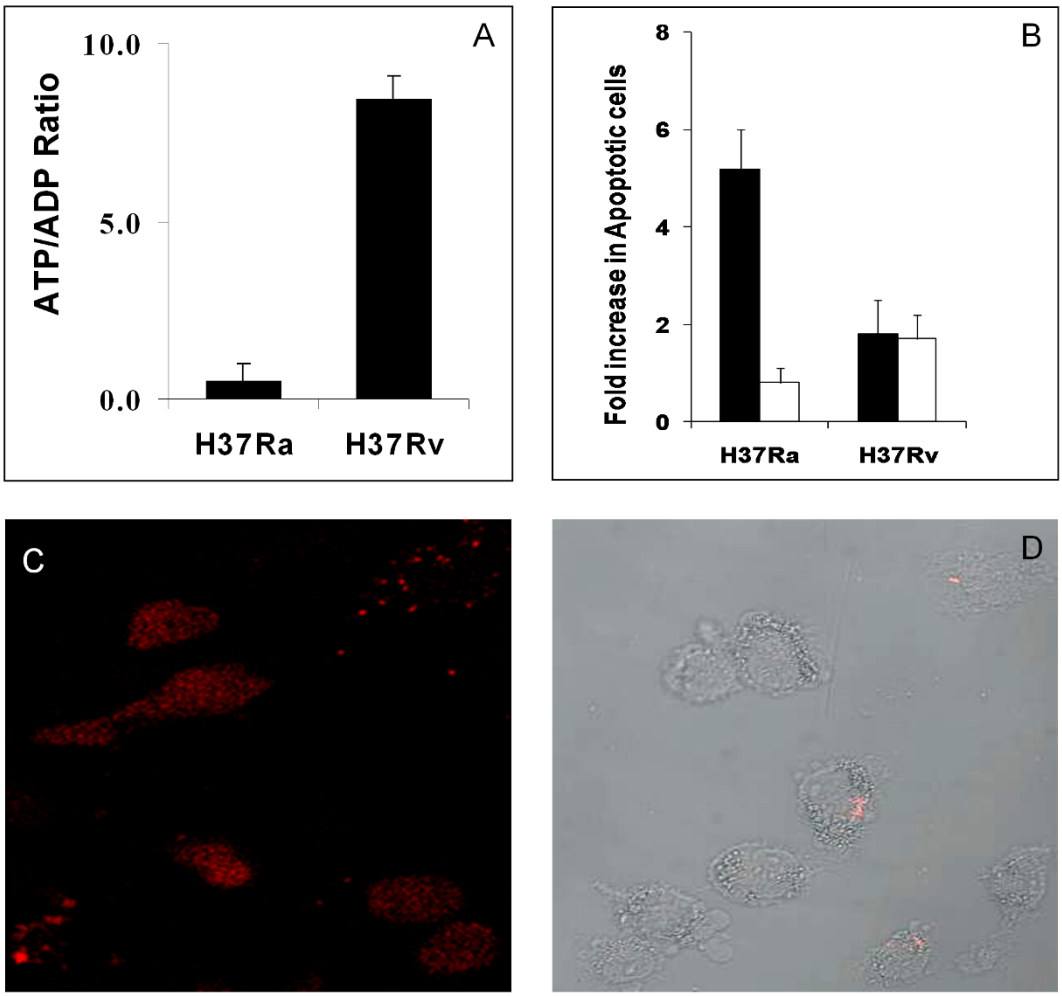


**Figure 4 | Differential effects of H37Ra versus H37Rv infection on mitochondrial function and the host cellular response.** Either uninfected cells, or cells infected with 24 hrs with either H37Ra or with H37Rv were processed for the quantification of cellular ATP/ADP ratios as described in Methods. In a separate experiment, cells were infected for a 72 hr period and the extent of death induced, over that in uninfected cells, was determined by the TUNEL assay. These results are shown in panel B (filled bars). Also shown here are the effects of the pan-caspase inhibitor Z-VAD-FMK (50 μM, open bars, panel B), which was added at 48 hrs post-infection. Values in both cases are the mean (± S.D.) of three experiments. In a parallel experiment, we also probed the mode of infection-induced death by using the Apoptosis/Necrosis Detection Kit (Enzo Life Sciences). The fluorescence microscopy images in panel C show that cells infected with H37Ra were predominantly stained with Cyanin 3-labeled annexin-V. This is indicative of apoptotic death. In contrast, H37Rv-infected cells were largely negative for annexin-V staining, although some of them were found to take up the membrane impermeable nuclear probe 7-AAD. Panel D shows a merge of images for 7-AAD staining (pink), obtained by confocal microscopy, with the differential interference contrast images of cells in the same field.

requires the coordinated supply of phospholipids, and defined functions for this class of molecules is emerging in diverse processes such as energy production, membrane fusion, and regulation of apoptosis[33]. Thus the increase in ACSL1 levels could well contribute to the enhanced structural integrity and function of the mitochondria in H37Rv infected cells.

The Voltage-dependent anion-selective channel protein 2 (VDAC-2) is directly involved in the regulation of mitochondrial apoptosis[34]. More recent evidence suggests that it interacts with the proapototic protein BAK, a member of the BCL2 protein family, and thereby inhibits its oligomerization[34]. Oligomerization of BAK acts as a signal for the induction of apoptosis. Similarly, PRDX1 (Peroxiredoxin 1) also shares an anti-apoptotic role although this function is exercised by protecting mitochondria against oxidative stress. PRDX1 is primarily responsible for eliminating peroxides generated during metabolism[35].

ATAD3A, the ATPase family AAA domain containing 3A protein, is yet another important negative regulator of mitochondrial apoptosis. Silencing of ATAD3A gene expression in lung adenocarcinoma cells has been shown to enhance mitochondrial fragmentation[36]. Interestingly, this protein was found to be upregulated under conditions of cellular stress[36]. A particularly significant protein in the list in Table 1 is ATP50. This protein is a component of the FoF1 ATP synthase of mitochondria, and forms a part of the connector linking the F1 catalytic core with the Fo membrane proton channel domain[36]. It has been suggested that this protein may be involved in proton conductance between the two domains[37]. This is essential for the ATP synthase activity of the holoenzyme[37]. Thus, our finding that ATP50 levels are markedly enhanced in H37Rv-infected THP-1 cells would at least partially explain the findings in Figures 3 and 4A.

The set of proteins whose levels were suppressed in H37Rv-infected cells was composed of ATP5B, ATP5A1, OAS2, PRDX3, HADHA, and SQRDL (Table 1). ATP5A1 and ATP5B are the α and β subunits of the F1 component of the mitochondrial FoF1 ATP synthase[37]. These two subunits contribute the catalytic nucleotide binding sites of the F1 domain. The proton-motive force

Table 1 | Quantitative perturbations in the mitochondrial proteome following infection of THP-1 cells with either H37Ra or with H37Rv. Table lists the THP-1 cell mitochondrial proteins whose levels were affected by greater than 10-fold, relative to that in uninfected cells, following infection with either H37Ra or H37Rv. Here, ND denotes absence of that protein in cells infected with relevant Mtb strain, while the value of 100 indicates those proteins that were undetectable in uninfected cells. Further details are provided in the text

| | | | Ratio | |
|---|---|---|---|---|
| No. | Protein Identity | Accession # | H37Ra | H37Rv |
| 1 | ACSL4 | 060488 | 0.0121 | 0.3839 |
| 2 | ATP5B | P06576 | 0.8594 | ND |
| 3 | UQCRH | P07919 | 0.0121 | 0.584 |
| 4 | DLD | P09622 | 0.0121 | 7.143 |
| 5 | HCLS1 | P14317 | 1.544 | 23.6273 |
| 6 | ACAT1 | P24752 | 0.0121 | 0.3839 |
| 7 | ATP5A1 | P25705 | 1.4391 | ND |
| 8 | OAS2 | P29728 | 2.613 | ND |
| 9 | PRDX3 | P30048 | 100 | ND |
| 10 | ACSL1 | P33121 | 100 | 100 |
| 11 | HADHA | P40939 | 100 | ND |
| 12 | VDAC2 | P45880 | 1.7054 | 38.8317 |
| 13 | ATP5O | P48047 | 0.6105 | 11.5712 |
| 14 | PRDX1 | Q06830 | 1.3534 | 24.7977 |
| 15 | ATAD3A | Q9NV17 | ND | 100 |
| 16 | SQRDL | Q9Y6N5 | 11.7937 | ND |

generated by the electron transport chain cause F1 to go through a series of conformational changes that leads to ATP synthesis[37]. A *priori* then, the observed reduction in the level of these two proteins may appear to be contradictory to our finding that the ATP to ADP ratio is significantly enhanced in H37Rv-infected cells (see Fig. 4A). However it must be noted that, depending on the conditions, the catalytic subunits of F1 also drive the reverse reaction of ATP hydrolysis[37]. Of particular interest in this connection is the fact that some inhibitors that target the catalytic site in the F1 domain specifically prevent ATP hydrolysis but not its synthesis[38]. Thus the possibility that the altered stoichiometry between ATP50, and the ATP5A1 and the ATP5B subunits of F1 may exert a differential effect on the competing pathways of ATP synthesis versus hydrolysis cannot be ruled out.

OAS2 (2′-5′-oligoadenylate synthase 2) is an important protein that is linked to IFNγ-induced iNOS. The latter enzyme generates NO using arginine as a substrate and the IFNγ-mediated induction of iNOS has been shown to represent an important pathway by which intracellular mycobacteria are killed[39]. Further, NO also induces apoptosis of Mtb-infected macrophages[40]. The observed suppression of OAS2 protein levels can, therefore, be easily rationalized as a pro-survival mechanism activated by the virulent Mtb. Interestingly, downregulation of SQRDL - a mitochondrial sulfide:quinone oxidoreductase – can be expected to further contribute towards protecting the bacilli from the microbicidal effects of NO. SQRDL is primarily responsible for oxidizing H2S to sulfide[41]. In mammalian cells, H2S is generated through the activity of two pyridoxal phosphate-dependent enzymes: cistathione-γ-lyase (CSE) and cystathione-β-synthetase[41]. This H2S interacts with the peroxynitrite anion formed from the reaction between NO and superoxide[41], thereby effectively neutralizing the anti-microbial and pro-apoptotic effects of NO. Thus, a decrease in SQRDL levels can be expected to favor H2S accumulation, and the consequent quenching any NO activity that may be generated.

HADHA is the alpha subunit of the mitochondrial trifunctional protein that catalyzes beta-oxidation of long-chain fatty acids[42,43]. The implication of the downregulation of this protein by H37Rv, in terms of regulating the death versus survival of the host macrophage, is presently unclear. However, since host cellular lipids constitute the primary nutrient source for intracellular Mtb[44], inhibition of lipid catabolism may be relevant for facilitating survival of the mycobacteria. Finally, given that PRDX3 (Peroxiredoxin 3) shares the anti-oxidant properties of PRDX1, and detoxifies H2O2 to prevent apoptosis[45], the suppression of this protein in H37Rv-infected cells is somewhat puzzling. It will indeed be interesting to probe how the differential effects on PRDX1 versus PRDX3 impinge on regulating the host cellular response.

**Mitochondrial proteins affected by H37Ra infection.** Of the proteins whose levels were significantly affected by H37Ra infection, the downregulation of UQCRH, a subunit of the ubiquinol-cytochrome c reductase complex[46] is of particular interest. The parent enzyme is an important component of the respiratory chain and is involved in the reduction of molecular oxygen[46]. The decrease in levels of this protein therefore, is consistent with the observed induction of apoptosis in H37Ra-infected cells. ACSL4, a member of the Acyl-CoA synthetase long-chain family, converts free long-chain fatty acids into the fatty acyl-CoA esters. This conversion is a prerequisite for the biosynthesis of triglycerides, which then accumulate in the form of lipid bodies (LBs). Previous studies have shown that LB formation is critical for intracellular Mtb survival as they provide a privileged environment that protects the bacilli against the anti-microbial activities of the host cell[43,46]. The suppressed level of this protein would, therefore, imply increased killing of H37Ra inside macrophages. Indeed we have recently demonstrated that, relative to the situation with H37Rv, H37Ra-infected THP-1 cells display an attenuated LB response and that this diminished response is directly responsible for elimination of intracellular bacilli[47].

The concomitant suppression of ACAT1, an enzyme involved in LB biogenesis[48], is likely to further augment the inhibition of LB accumulation by the host macrophage, in response to H37Ra infection. This possibility is experimentally supported by our recent demonstration that either siRNA-mediated silencing, or pharmacological inhibition of ACATs, indeed prevents LB formation in Mtb infected THP-1 cells[47].

The downregulation of DLD or dihydrolipoamide dehydrogenase is also of interest as this protein is a constituent of the pyruvate dehydrogenase complex, the alpha-ketoglutarate dehydrogenase complex, and the branched-chain alpha-keto acid dehydrogenase complex[49]. Thus, at one level, suppression of this protein is likely to negatively impact on the Citric acid cycle, thereby also inhibiting energy production by the cell. In addition, amino acid metabolism is also likely to be impaired[49]. Interestingly, in similarity with the situation for H37Rv infection, ACSL1 levels were also markedly induced in H37Ra-infected cells. As discussed earlier upregulation of this protein is likely to facilitate increased production of fatty acyl-CoA. The implication of this, in the context of the cellular outcome of infection with H37Ra, is not clear. It may be possible that, under conditions where levels of ACSL4 and ACAT1 are diminished, the effect of ACSL1 may be to shunt free fatty acids into the beta-oxidation pathway as a stress response of the host cell to infection.

As perhaps may be expected, we also noted instances where the virulent and the avirulent Mtb strain exercised opposing effects on mitochondrial protein levels. Thus, whereas the anti-apoptotic protein ATAD3A was found to be upregulated in H37Rv infected cells it was, however, significantly downregulated following H37Ra infection (Table 1). Conversely, while the amounts of HADHA, SQRDL and PRDX3 were reduced after infection with H37Rv, they were induced to markedly higher levels in H37Ra infected cells (Table 1). Given its role in NO detoxification as discussed above, the induction of SQRDL may reflect an anti-microbial response of the host cell that – unlike H37Rv - the avirulent mycobacterium is

unable to counter. The enhancement in HADHA suggests increased beta-oxidation of fatty acids in H37Ra infected cells and it is possible that this activity may be additionally complemented by the increase in ASCL1 levels. If such a hypothesis indeed proves to be true then this would indicate an interesting shift in host cell fatty acid metabolism pathways, following infection with either a virulent or an avirulent strain of Mtb. Whereas cells infected with H37Rv appear to show a bias towards converting free fatty acids into triglycerides and consequent LB formation, H37Ra infection seems to activate pathways involved in fatty acid catabolism.

Finally, the observed upregulation of the anti-oxidant protein PRDX3 levels by H37Ra is somewhat puzzling and the functional implications are not immediately evident. In view of its function in scavenging $H_2O_2$, one would expect this protein to contribute towards protection from apoptosis. It is, however, possible that this function may be overridden by the other pro-apoptotic signals activated in cells infected with avirulent Mtb. Alternatively, the possibility that PRDX3 may act through additional, as yet undefined, pathways cannot be ruled out. In either event it is intriguing that this protein is regulated in an opposite manner depending upon whether the macrophage is infected with a virulent or an avirulent strain of Mtb.

## Discussion

Following uptake, the ability to survive and persist in the alveolar macrophages is a key property that describes Mtb virulence. An initial phase of growth within these cells is essential for the establishment of a productive infection. This aspect was demonstrated by experiments where mice depleted of alveolar macrophages were relatively better protected from Mtb infection, although their susceptibility to infection with *Streptococcus pneumonia* was markedly enhanced[50]. These findings suggest that, in spite of the potent array of anti-microbial activities that this cell type possesses, virulent Mtb is able to successfully coopt the intracellular milieu of the macrophage as a protective survival niche that at least facilitates stabilization of the infection. Studies from several laboratories show that this occurs through the active suppression of the host cell pathways.

In response to an infection, a prominent defense response of the macrophage is to activate pathways leading to programmed cell death[51]. This provides a mechanism wherein the host cell can contain the infection, and then eliminate it before it can further disseminate in the body[21,52–54]. Apoptosis is also often accompanied by the expression of anti-inflammatory cytokines, which then limit the tissue damage that may occur. In addition to this orchestrated elimination of infected cells, the packaging of pathogen-derived molecules into apoptotic bodies provides an efficient pathway for delivery of antigens to immature dendritic cells, thus leading to the activation of an adaptive immune response[55,56].

That prevention of host macrophage apoptosis represents an important survival pathway of Mtb is evident from earlier observations that infection with attenuated strains of Mtb such as H37Ra or *M. bovis BCG* rapidly induced innate macrophage apoptosis even at low multiplicities of infection[21,53]. In contrast, virulent strains inhibit this apoptotic response. An important outstanding question that persists, however, is the nature of perturbations that virulent Mtb exercise on the host cell, in order to suppress the early activation of apoptotic pathways. While the modulations exerted on the penultimate stages apoptosis have now been uncovered[22], little is known on whether Mtb also perturbs the early pathways that initiate this process.

We, therefore, undertook the present study to explore this aspect. A thorough examination of this issue clearly requires an exhaustive and detailed analysis. Therefore, the present work was designed more as an exploratory investigation, to establish whether the differential host cellular outcomes to either H37Ra or H37Rv infection could be captured at the level of early modulations in mitochondrial function. This was because activation of intrinsic cell death pathways normally initiate from perturbations in integrity and function of this organelle.

Consistent with expectations, THP-1 cells infected with H37Ra rapidly underwent apoptosis, whereas this response was significantly attenuated in cells infected with H37Rv. Of particular interest though was the fact these distinct outcomes were indeed marked soon after infection, at the level of structural and functional perturbations in the mitochondria of the host cell. Thus, while mitochondria in cells infected with either H37Ra or with H37Rv showed distinct alterations in ultrastructure, these changes also correlated with differences in function when measured either at the level of the mitochondrial membrane potential, or at that of ATP synthesis. These findings, therefore, prompted us to explore whether the observed variations could be explained through regulation in at least some fraction of the mitochondrial proteome.

Although significantly limited in scope the results of our quantitative proteomic analysis, nonetheless, provide a ready rationalization for the distinct consequences of H37Ra versus H37Rv infection. Thus for example, the increased ATP production by mitochondria in H37Rv-infected cells was reflected, at the functional level, by the specific induction of the ATP50 subunit of the mitochondrial $F_oF_1$ ATP synthase in these cells. In contrast, decreased functional activity of these organelles in H37Ra-infected cells could at least partially be accounted for by the reduction in levels of UQCRH and DLD. As a result, activity of both the citric acid cycle and the associated electron transport chain are likely to be hampered.

Importantly, our results also yielded a preliminary glimpse into the mechanisms involved in the H37Rv-dependent suppression of cellular apoptosis. Thus, the anti-apoptotic activities of VDAC2, ATAD3, and PRDX1 – all of which are markedly upregulated - would at least partly be responsible for this effect. Such an interpretation is supported by the fact that these proteins were not induced upon infection with H37Ra. On the contrary, level of the ATAD3 protein was significantly reduced in the latter case. The loss of the apoptosis-inhibitory function of this protein may, therefore, serve to further facilitate activation of cell death pathways in H37Ra-infected cells.

Yet another notable aspect of our results was the clear evidence of suppression of host bactericidal pathways by virulent Mtb. Indeed the efficiency with which this is likely achieved was underscored by the simultaneous downregulation of both the OAS2 and SQRDL proteins. As a result, while production of NO by the host macrophage is likely attenuated through OAS2 suppression, any residual NO would then be further quenched due to the diminished activity of SQRDL. Previous studies have shown that the macrophage NO response constitutes at least a dominant mechanism for the killing of intracellular Mtb[40]. No such suppressive effects were, however, seen in H37Ra infected cells. Rather SQRDL levels were augmented in this case implying at least some degree of success for the macrophage in activating an anti-microbial response, when the pathogen was an avirulent Mtb strain.

The Mtb virulence-specific distinctions in perturbations induced in the host lipid metabolic pathways is also of particular interest. Previous studies have shown that infection of macrophages with virulent Mtb causes them to differentiate into 'foamy' macrophages (FMs)[57]. These FMs are characterized by the accumulation of lipid bodies (LBs)[44]. Interestingly, Mtb containing phagosomes have been shown to migrate towards these LBs and, eventually engulf them[57]. Following this, the mycobacteria are then released into the lipid bodies. This encapsulation serves to protect the bacilli against the host anti-microbial response and, thereby, provides a niche for long-term persistence[43,46]. Interestingly, we have recently shown that only virulent Mtb strains can induce LBs in the host macrophage, and that both avirulent and attenuated strains lack this capability[47]. In our present data, the induction of phospholipid synthesis through upregulation of ACSL1, with the simultaneous reduction in fatty acid

degradation due to reduced HADHA levels, are probably at least some of the factors that contribute to increase LB biogenesis. On the other hand, clear evidence of suppression of LB induction pathways by the host macrophage was seen in H37Rv infected cells. This was evidenced at the level of suppression of both ACSL4 and ACAT1. This inhibitory effect is then probably further augmented through the catabolic depletion of the free fatty acid pool, which is likely facilitated by the increased levels of HADHA. Importantly here, the resultant depletion of the protective LB cover can be expected to sensitize H37Ra to the bactericidal effects of NO.

It is, therefore, clear from the above results that an interrogation of the mitochondrial proteome indeed provides insights into the molecular interplay between the host and the Mtb pathogen. Importantly, our strategy of comparing between H37Ra versus H37Rv infection also proved useful as it yielded a glimpse into the mechanisms by which virulent Mtb modulates host cellular responses. Although admittedly still of a preliminary nature, our results also underscore the integrated nature of the effects that H37Rv exercises on the host macrophage. Thus, early inhibition of pathways leading to both apoptosis and NO induction, coupled with the activation of LB formation, collectively ensure stable persistence of the bacilli in the intracellular environment. The study, therefore, highlights the utility of performing a more comprehensive examination of the Mtb-induced changes in the host cell mitochondrial proteome. Importantly, a temporal profiling of these changes - as a function of the duration of infection - can be expected to yield novel and important information on the mechanisms that drive adaptive equilibration of virulent Mtb within the macrophage.

## Methods

**Cell culture and infection.** THP-1 cells were cultured in RPMI-1640 supplemented with 10% FCS and maintained at between 2 – 10 × $10^5$ cells per ml at 37°C in a humidified, 5% $CO_2$ atmosphere. Cells were differentiated with PMA (30 ng/ml) for 48 hr. They were then infected with either H37Ra or with H37Rv at an MOI of 10 and any residual extra-cellular bacteria then removed through amikacin treatment as previously described[58].

**Transmission electron microscopy and 3D imaging.** Cells were processed for TEM as described earlier[59]. Briefly, uninfected or infected THP-1 cells were washed twice with 100 nM sodium cacodylate buffer (pH, 7.4) and fixed with 3% Glutaraldehyde (Sigma) for 30 min at room temperature. Fixed cells were then scraped off using a rubber policeman, transferred to microcentrifuge tubes, and stored overnight at 4°C. Post-fixation was done with 0.1% osmium tetroxide for 1 hr at room temperature, then dehydrated through graded alcohol series, and embedded in EPON 812 (Polysciences, USA). Blocks were polymerized at 60°C in a dry heat oven for 3–4 days. Ultrathin sections of 80–100 mm were cut using a diamond knife (Diatome) in an ultramicrotome (Ultracut R, Leica), and collected on 400-mesh size copper grids. Sections were stained using uranyl acetate for 10 min and contrasted with Reynold's lead citrate for 2 min at room temperature. Imaging was done under 80 and 100 KeV operating voltages of a transmission electron microscope (Technai 12 Biotwin TM, FEI Co., The Netherlands). Images were recorded digitally using a side-mounted 2 k × 2 k CCD camera (SIS, Germany).

For electron tomography, specimen grids were mounted on a FEI single-axis high-tilt tomography holder and a tilt-series of the selected area collected over ±65° using 1° tilt increments. The tomography data sets were collected using automated tomography software (FEI Co., The Netherlands) and data processed using the Inspect 3D (FEI Co.) software. The 3D visualization was done using the AMIRA package (Visage Imaging, France).

**Assays for mitochondrial membrane potential, ATP/ADP ratio, and cellular apoptosis.** The mitochondrial membrane potential was measured using the Mitochondrial staining kit for mitochondrial potential changes detection (Sigma-Aldrich), as per the manufacturer's protocol. The cellular ATP/ADP ratio was determined from lysates generated at 24 hr post-infection. The ADP/ATP ratio assay kit (Abcam) was used for this purpose, according to recommended protocol. For the TUNEL assay we employed the In Situ Cell Death Detection Kit from Roche and followed the protocol recommended by the manufacturer.

**SILAC labeling and isolation of mitochondria.** THP-1 cells were maintained in the appropriate heavy labeled medium for 5 passages prior to differentiation with PMA and subsequent infection. We used Lys-6 for cells to be infected with H37Ra, and Lys-8 for those to be infected with H37Rv. A parallel set of uninfected cells was maintained in normal medium. At 24 hr post-infection, equal numbers of uninfected, H37Ra-infected, and H37Rv-infected cells were pooled. This cell pool was then employed for isolation of mitochondria by using the Mitochondrial isolation kit (Sigma) and strictly following the protocol recommended by the manufacturer. The suspension of isolated mitochondria was lyophilized, and then re-suspended in 100 nM ammonium bicarbonate buffer. The proteins were then subjected to denaturation and reductive alkylation prior to digestion with a combination of Lys-C and trypsin. A schematic of the overall protocol is shown in Supplementary Figure 1. The peptides thus obtained were analyzed by 2D-LC-MS/MS as described below.

**2D LC-MS/MS Analysis.** SILAC-labeled peptide mixtures were separated by two-dimensional liquid chromatography and analyzed by LC-MALDI MS/MS. The labeled peptide mixture was separated by off-line strong cation-exchange (SCX) chromatography using HPLC with a UV detector (1200 series, Quaternary pumps, Agilent). The labeled samples (100 μg) were reconstituted in SCX low ionic strength buffer (5 mM ammonium formate, 30% acetonitrile (ACN)) and injected onto a PolyLC Polysulfethyl A Zorbax 300SCX column, 5 μm (2.1 mm × 150 mm, Agilent). Peptides were eluted with increasing salt gradient of 5 mM ammonium formate, 30% ACN to 500 mM ammonium formate, 30% ACN over 40 mins. Seventeen fractions 800 μL each were collected at a flow rate of 400 μL/min according to UV trace at 220 nm. Peptide samples after drying were further fractionated offline on a Tempo nano-LC and spotted on MALDI plates.

The partially purified peptide mixtures were analyzed by reverse-phase liquid chromatography (Tempo nano LC from Applied Biosystems, Foster City, CA) offline coupled to ABI 5800 Proteomics Analyzer MALDI-TOF/TOF mass spectrometer, (Applied Biosystems, Foster City, CA). Each fraction was reconstituted in 15 μl of 1A buffer (98% water, 2% ACN and 0.1% TFA) and 12 μl was picked up by autosampler and directly loaded on to LC tempo column (Chromolith monolithic capillary, RP C18, 150 × 0.1 mm) and separated using 50 min. gradient: 5% ACN to 50% ACN. The column eluates containing peptides were mixed with 5 mg/ml CHCA (α-cyano-4 hydroxy cinnamic acid) matrix in 85% acetonitrile (ACN), 0.1% Trifluoroacetic acid (TFA), and the resulting solution was spotted at a 1.5 μl/min flow rate on 1232 well (44 × 28) LC-MALDI stainless steel plate. Protein identification was performed on an ABSCIEX MALDI- TOF/TOF™ 5800 Analyzer (AB SCIEX, Foster City, CA) equipped with a neodymium: yttrium-aluminum-garnet laser (laser wavelength was 349 nm). The TOF/TOF calibration mixtures of reference peptides (des-Arg1-bradykinin, MH = 904.468 Da; Angiotensin I, MH = 1296.685 Da; Glu1-fibrinopeptide, MH = 1570.677 Da; ACTH, MH = 2093.087 Da; ACTH, MH = 2465.199 Da; ACTH) were used to calibrate the spectrum to a mass tolerance within 50 ppm. For MS mode, peptide mass maps were acquired in positive reflection mode, and 800 – 4000 m/z mass range was used with 1500 laser shots per spectrum. The PMF peak detection criteria used include minimum signal-to-noise (S/N) of 10, local noise window width mass/charge (m/z) of 250, and minimum full-width half-maximum (bins) of 1. A maximum of 30 precursors per spot with a minimum signal/noise ratio of 25 were selected for MS/MS analysis using ambient air as the collision gas with medium pressure of $10^{-6}$ Torr. Energy of 1 KV was used for collision-induced dissociation (CID), and 4000 acquisitions were accumulated for each MS/MS spectrum with dynamic exclusion mode of captured peptides. The peak detection criteria used were minimum S/N of 5, local noise window width (m/z) of 200, and minimum full-width half-maximum (bins) of 2.9. The Interpretation for MS/MS analysis includes the exclusion of contaminant m/z peaks originating from human keratin, trypsin auto-digestion and matrix. The SILAC-labeled samples were analyzed twice on the same platform.

**Database Search and Relative Quantification.** All automatic data analysis (MS and MS/MS) and database searching were conducted against the Uniprot database (version 04-25-2012) using the ProteinPilot™ software (version 4.0, revision 148085, Applied Biosystems) with the Paragon™ method utilizing the following search parameters: *Homosapiens* as species, trypsin as enzyme (one missed cleavage allowed), with fixed modification of Methyl methanethiosulphonate (MMTS) - labeled cysteine parameter enabled, SILAC-Lys6 and Lys8 labeled as sample type and the 'Search Effort' parameter 'Thorough ID', which provides a broad search of various protein modifications and multiple mass cleavages, were chosen. The raw peptide identification results from the Paragon™ Algorithm (Applied Biosystems) searches were further processed by the Pro Group™ Algorithm (Applied Biosystems) within the ProteinPilot software before final display[60].

The parameters used for identification and quantification of differentially expressed proteins includes: 1) Threshold of 5% accepted Global False discovery rate (G-FDR) proteins; 2) At least more than one peptide with 95% confidence for identification and at least two peptides for the relative expression[60] (see Supplementary Fig. 2). The false positive rates of the aforementioned filter criteria were all below 5%, estimated by using an individual reversed (decoy) sequence database. In brief, false positive rates were calculated by dividing the number of decoy hits by that of hits acquired in search against forward sequence database[61]. Samples from two biological replicates (set 1 and set 2) were analyzed and the collective data identified a total of 1299 unique human proteins. These proteins are listed in Supplementary Table 1. We validated the quantitative inferences obtained from the SILAC labeling by also performing an RT-PCR analysis for the expression levels of genes coding for a select list of proteins listed in Table 1. As shown in Supplementary Figure 3, the infection-induced differences in expression levels of these genes are broadly consistent with the profiles obtained in Table 1.

1. Koul, A., Herget, T., Klebl, B. & Ullrich, A. Interplay between mycobacteria and host signalling pathways. *Nature reviews* **2**, 189–202 (2004).

2. Kaufmann, S. H., Cole, S. T., Mizrahi, V., Rubin, E. & Nathan, C. Mycobacterium tuberculosis and the host response. *The Journal of experimental medicine* **201**, 1693–1697 (2005).
3. Meena, L. S. & Rajni Survival mechanisms of pathogenic Mycobacterium tuberculosis H37Rv. *The FEBS journal* **277**, 2416–2427 (2010).
4. Cooper, A. M. Cell-mediated immune responses in tuberculosis. *Annual review of immunology* **27**, 393–422 (2009).
5. Robinson, N. A., Lapic, S., Welter, J. F. & Eckert, R. L. S100A11, S100A10, annexin I, desmosomal proteins, small proline-rich proteins, plasminogen activator inhibitor-2, and involucrin are components of the cornified envelope of cultured human epidermal keratinocytes. *The Journal of biological chemistry* **272**, 12035–12046 (1997).
6. Molloy, A., Laochumroonvorapong, P. & Kaplan, G. Apoptosis, but not necrosis, of infected monocytes is coupled with killing of intracellular bacillus Calmette-Guerin. *The Journal of experimental medicine* **180**, 1499–1509 (1994).
7. Davis, J. M. & Ramakrishnan, L. The role of the granuloma in expansion and dissemination of early tuberculous infection. *Cell* **136**, 37–49 (2009).
8. Ramakrishnan, L. Revisiting the role of the granuloma in tuberculosis. *Nat Rev Immunol* **12**, 352–366(2012).
9. Sly, L. M., Hingley-Wilson, S. M., Reiner, N. E. & McMaster, W. R. Survival of Mycobacterium tuberculosis in host macrophages involves resistance to apoptosis dependent upon induction of antiapoptotic Bcl-2 family member Mcl-1. *J Immunol* **170**, 430–437 (2003).
10. Simeone, R. *et al.* Phagosomal rupture by Mycobacterium tuberculosis results in toxicity and host cell death. *PLoS pathogens* **8**, e1002507 (2012).
11. Park, J. S., Tamayo, M. H., Gonzalez-Juarrero, M., Orme, I. M. & Ordway, D. J. Virulent clinical isolates of Mycobacterium tuberculosis grow rapidly and induce cellular necrosis but minimal apoptosis in murine macrophages. *Journal of leukocyte biology* **79**, 80–86 (2006).
12. Lee, J., Remold, H. G., Ieong, M. H. & Kornfeld, H. Macrophage apoptosis in response to high intracellular burden of Mycobacterium tuberculosis is mediated by a novel caspase-independent pathway. *J Immunol* **176**, 4267–4274 (2006).
13. O'Sullivan, M. P., O'Leary, S., Kelly, D. M. & Keane, J. A caspase-independent pathway mediates macrophage cell death in response to Mycobacterium tuberculosis infection. *Infection and immunity* **75**, 1984–1993 (2007).
14. Briken, V. & Miller, J. L. Living on the edge: inhibition of host cell apoptosis by Mycobacterium tuberculosis. *Future microbiology* **3**, 415–422 (2008).
15. Welin, A., Eklund, D., Stendahl, O. & Lerm, M. Human macrophages infected with a high burden of ESAT-6-expressing M. tuberculosis undergo caspase-1- and cathepsin B-independent necrosis. *PloS one* **6**, e20302 (2011).
16. Lee, J., Repasy, T., Papavinasasundaram, K., Sassetti, C. & Kornfeld, H. Mycobacterium tuberculosis induces an atypical cell death mode to escape from infected macrophages. *PloS one* **6**, e18367 (2011).
17. Ciaramella, A. *et al.* Induction of apoptosis and release of interleukin-1 beta by cell wall-associated 19-kDa lipoprotein during the course of mycobacterial infection. *The Journal of infectious diseases* **190**, 1167–1176 (2004).
18. Basu, S. *et al.* Execution of macrophage apoptosis by PE_PGRS33 of Mycobacterium tuberculosis is mediated by Toll-like receptor 2-dependent release of tumor necrosis factor-alpha. *The Journal of biological chemistry* **282**, 1039–1050 (2007).
19. Sanchez, A. *et al.* Mycobacterium tuberculosis 38-kDa lipoprotein is apoptogenic for human monocyte-derived macrophages. *Scandinavian journal of immunology* **69**, 20–28 (2009).
20. Sohn, H. *et al.* Targeting of Mycobacterium tuberculosis heparin-binding hemagglutinin to mitochondria in macrophages. *PLoS pathogens* **7**, e1002435(2011).
21. Keane, J. *et al.* Infection by Mycobacterium tuberculosis promotes human alveolar macrophage apoptosis. *Infection and immunity* **65**, 298–304 (1997).
22. Gan, H. *et al.* Mycobacterium tuberculosis blocks crosslinking of annexin-1 and apoptotic envelope formation on infected macrophages to maintain virulence. *Nature immunology* **9**, 1189–1197 (2008).
23. Schwartzman, R. A. & Cidlowski, J. A. Apoptosis: the biochemistry and molecular biology of programmed cell death. *Endocrine reviews* **14**, 133–151 (1993).
24. Wang, C. & Youle, R. J. The role of mitochondria in apoptosis*. *Annual review of genetics* **43**, 95–118 (2009).
25. Sanchez-Alcazar, J. A., Ault, J. G., Khodjakov, A. & Schneider, E. Increased mitochondrial cytochrome c levels and mitochondrial hyperpolarization precede camptothecin-induced apoptosis in Jurkat cells. *Cell death and differentiation* **7**, 1090–1100 (2000).
26. Karbowski, M. & Youle, R. J. Dynamics of mitochondrial morphology in healthy cells and during apoptosis. *Cell death and differentiation* **10**, 870–880 (2003).
27. Deng, L. *et al.* Hepatitis C virus infection induces apoptosis through a Bax-triggered, mitochondrion-mediated, caspase 3-dependent pathway. *Journal of virology* **82**, 10375–10385 (2008).
28. van der Bliek, A. M. Fussy mitochondria fuse in response to stress. *The EMBO journal* **28**, 1533–1534 (2009).
29. Chen, M., Gan, H. & Remold, H. G. A mechanism of virulence: virulent Mycobacterium tuberculosis strain H37Rv, but not attenuated H37Ra, causes significant mitochondrial inner membrane disruption in macrophages leading to necrosis. *J Immunol* **176**, 3707–3716 (2006).
30. Harsha, H. C., Molina, H. & Pandey, A. Quantitative proteomics using stable isotope labeling with amino acids in cell culture. *Nature protocols* **3**, 505–516 (2008).
31. Suzuki, H. *et al.* Structure and regulation of rat long-chain acyl-CoA synthetase. *The Journal of biological chemistry* **265**, 8681–8685 (1990).
32. Li, L. O. *et al.* Overexpression of rat long chain acyl-coa synthetase 1 alters fatty acid metabolism in rat primary hepatocytes. *The Journal of biological chemistry* **281**, 37246–37255 (2006).
33. Osman, C., Voelker, D. R. & Langer, T. Making heads or tails of phospholipids in mitochondria. *The Journal of cell biology* **192**, 7–16 (2011).
34. Cheng, E. H., Sheiko, T. V., Fisher, J. K., Craigen, W. J. & Korsmeyer, S. J. VDAC2 inhibits BAK activation and mitochondrial apoptosis. *Science* (*New York, N.Y.*) **301**, 513–517 (2003).
35. Bast, A., Fischer, K., Erttmann, S. F. & Walther, R. Induction of peroxiredoxin I gene expression by LPS involves the Src/PI3K/JNK signalling pathway. *Biochimica et biophysica acta* **1799**, 402–410 (2010).
36. Fang, H. Y. *et al.* ATPase family AAA domain-containing 3A is a novel anti-apoptotic factor in lung adenocarcinoma cells. *Journal of cell science* **123**, 1171–1180 (2010).
37. Ueno, H., Suzuki, T., Kinosita, K. Jr. & Yoshida, M. ATP-driven stepwise rotation of FoF1-ATP synthase. *Proceedings of the National Academy of Sciences of the United States of America* **102**, 1333–1338 (2005).
38. Lang, D. R. & Racker, E. Effects of quercetin and F1 inhibitor on mitochondrial ATPase and energy-linked reactions in submitochondrial particles. *Biochimica et biophysica acta* **333**, 180–186 (1974).
39. Ismail, N., Olano, J. P., Feng, H. M. & Walker, D. H. Current status of immune mechanisms of killing of intracellular microorganisms. *FEMS microbiology letters* **207**, 111–120 (2002).
40. Herbst, S., Schaible, U. E. & Schneider, B. E. Interferon gamma activated macrophages kill mycobacteria by nitric oxide induced apoptosis. *PloS one* **6**, e19105 (2011).
41. Li, L., Bhatia, M. & Moore, P. K. Hydrogen sulphide--a novel mediator of inflammation? *Current opinion in pharmacology* **6**, 125–129 (2006).
42. Aoyama, T., Wakui, K., Orii, K. E., Hashimoto, T. & Fukushima, Y. Fluorescence in situ hybridization mapping of the alpha and beta subunits (HADHA and HADHB) of human mitochondrial fatty acid beta-oxidation multienzyme complex to 2p23 and their evolution. *Cytogenetics and cell genetics* **79**, 221–224 (1997).
43. Kageyama, T. *et al.* HADHA is a potential predictor of response to platinum-based chemotherapy for lung cancer. *Asian Pac J Cancer Prev* **12**, 3457–3463 (2011).
44. Daniel, J., Maamar, H., Deb, C., Sirakova, T. D. & Kolattukudy, P. E. Mycobacterium tuberculosis uses host triacylglycerol to accumulate lipid droplets and acquires a dormancy-like phenotype in lipid-loaded macrophages. *PLoS pathogens* **7**, e1002093 (2011).
45. Nonn, L., Berggren, M. & Powis, G. Increased expression of mitochondrial peroxiredoxin-3 (thioredoxin peroxidase-2) protects cancer cells against hypoxia and drug-induced hydrogen peroxide-dependent apoptosis. *Mol Cancer Res* **1**, 682–689 (2003).
46. Megehee, J. A., Hosler, J. P. & Lundrigan, M. D. Evidence for a cytochrome bcc-aa3 interaction in the respiratory chain of Mycobacterium smegmatis. *Microbiology (Reading, England)* **152**, 823–829 (2006).
47. Singh, V., Jamwal, S., Jain, R., Verma, P., Gokhale, R. & Rao, K. V. S. Intracellular adaptation of Mycobacterium tuberculosis involves targeted recalibration of lipid homeostasis in macrophages (2012).
48. Sakashita, N. *et al.* Cholesterol loading in macrophages stimulates formation of ER-derived vesicles with elevated ACAT1 activity. *Journal of lipid research* **51**, 1263–1272 (2010).
49. Venugopal, A. *et al.* Virulence of Mycobacterium tuberculosis depends on lipoamide dehydrogenase, a member of three multienzyme complexes. *Cell host & microbe* **9**, 21–31 (2011).
50. Knapp, S. *et al.* Alveolar macrophages have a protective antiinflammatory role during murine pneumococcal pneumonia. *American journal of respiratory and critical care medicine* **167**, 171–179 (2003).
51. Roulston, A., Marcellus, R. C. & Branton, P. E. Viruses and apoptosis. *Annual review of microbiology* **53**, 577–628 (1999).
52. Lee, J., Hartman, M. & Kornfeld, H. Macrophage apoptosis in tuberculosis. *Yonsei medical journal* **50**, 1–11 (2009).
53. Riendeau, C. J. & Kornfeld, H. THP-1 cell apoptosis in response to Mycobacterial infection. *Infection and immunity* **71**, 254–259 (2003).
54. Oddo, M. *et al.* Fas ligand-induced apoptosis of infected human macrophages reduces the viability of intracellular Mycobacterium tuberculosis. *J Immunol* **160**, 5448–5454 (1998).
55. Schaible, U. E. *et al.* Apoptosis facilitates antigen presentation to T lymphocytes through MHC-I and CD1 in tuberculosis. *Nature medicine* **9**, 1039–1046 (2003).
56. Winau, F. *et al.* Apoptotic vesicles crossprime CD8 T cells and protect against tuberculosis. *Immunity* **24**, 105–117 (2006).
57. Peyron, P. *et al.* Foamy macrophages from tuberculous patients' granulomas constitute a nutrient-rich reservoir for M. tuberculosis persistence. *PLoS pathogens* **4**, e1000204 (2008).
58. Kumar, D. *et al.* Genome-wide analysis of the host intracellular network that regulates survival of Mycobacterium tuberculosis. *Cell* **140**, 731–743 (2010).

59. L.D., B. J. A. R. Preparation for transmission electron microscopy. In: Electron Microscopy, Principles and Techniques for Biologists. (Jones and Bartlett Publishers, Boston USA, 1992).
60. Shilov, I. V. *et al*. The Paragon Algorithm, a next generation search engine that uses sequence temperature values and feature probabilities to identify peptides from tandem mass spectra. *Mol Cell Proteomics* **6**, 1638–1655 (2007).
61. Peng, J., Elias, J. E., Thoreen, C. C., Licklider, L. J. & Gygi, S. P. Evaluation of multidimensional chromatography coupled with tandem mass spectrometry (LC/LC-MS/MS) for large-scale protein analysis: the yeast proteome. *Journal of proteome research* **2**, 43–50 (2003).

## Acknowledgements

We thank Ritu Jain for assistance with the confocal microscopy experiments and Varsha Sirohi is acknowledged for help with mitochondrial purification. This work was funded by a grant to KVSR from the Department of Biotechnology, Govt. of India.

## Author contributions

S.J., M.K.M. and A.B. performed the experiments and analyzed the data. H.N.M., K.V.S.R. and V.M. analyzed the data. K.V.S.R. and V.M. wrote the paper.

## Additional information

**Supplementary information** accompanies this paper at http://www.nature.com/scientificreports

**Competing financial interests:** The authors declare no competing financial interests.



**How to cite this article:** Jamwal, S. *et al*. Characterizing virulence-specific perturbations in the mitochondrial function of macrophages infected with *mycobacterium tuberculosis*. *Sci. Rep.* **3**, 1328; DOI:10.1038/srep01328 (2013).